

Photodissociation chemistry footprints in the Starburst galaxy NGC 253

Sergio Martín

Harvard-Smithsonian Center for Astrophysics, 60 Garden St., 02138, Cambridge, MA, USA

`smartin@cfa.harvard.edu`

J. Martín-Pintado

Centro de Astrobiología (CSIC-INTA), Ctra de Torrejón a Ajalvir, km 4, 28850 Torrejón
de Ardoz, Madrid, Spain

and

S. Viti

Physics and Astronomy Department, University College London, Gower Street, London,
WC1E 6BT, UK

Received _____; accepted _____

ABSTRACT

UV radiation from massive stars is thought to be the dominant heating mechanism of the nuclear ISM in the late stages of evolution of starburst galaxies, creating large photodissociation regions (PDRs) and driving a very specific chemistry. We report the first detection of PDR molecular tracers, namely HOC^+ , and CO^+ , and confirm the detection of the also PDR tracer HCO towards the starburst galaxy NGC 253, claimed to be mainly dominated by shock heating and in an earlier stage of evolution than M 82, the prototypical extragalactic PDR. Our CO^+ detection suffers from significant blending to a group of transitions of $^{13}\text{CH}_3\text{OH}$, tentatively detected for the first time in the extragalactic interstellar medium. These species are efficiently formed in the highly UV irradiated outer layers of molecular clouds, as observed in the late stage nuclear starburst in M 82. The molecular abundance ratios we derive for these molecules are very similar to those found in M 82. This strongly supports the idea that these molecules are tracing the PDR component associated with the starburst in the nuclear region of NGC 253. The presence of large abundances of PDR molecules in the ISM of NGC 253, which is dominated by shock chemistry, clearly illustrates the potential of chemical complexity studies to establish the evolutionary state of starbursts in galaxies. A comparison with the predictions of chemical models for PDRs shows that the observed molecular ratios are tracing the outer layers of UV illuminated clouds up to two magnitudes of visual extinction. We combine the column densities of PDR tracers reported in this paper with those of easily photodissociated species, such as HNCO , to derive the fraction of material in the well shielded core relative to the UV pervaded envelopes. Chemical models, which include grain formation and photodissociation of HNCO , support the scenario of a photo-dominated chemistry as an explanation to the abundances of the

observed species. From this comparison we conclude that the molecular clouds in NGC 253 are more massive and with larger column densities than those in M 82, as expected from the evolutionary stage of the starbursts in both galaxies.

Subject headings: galaxies: abundances — galaxies: ISM — galaxies: starburst — galaxies: individual(NGC 253)

1. Introduction

Intense UV radiation from massive stars is one of the main mechanisms responsible for the heating of the interstellar medium in the nuclear region of starburst galaxies. This mechanism is particularly important in the latest stages of starburst (SB) galaxies where the newly formed massive star clusters are responsible for creating large photodissociation regions (PDRs). This is the case for the prototypical SB galaxy M 82, where the large observed abundances of molecular species such as HCO, HOC⁺, CO⁺, and H₃O⁺ are claimed to be probes of the high ionization rates in large PDRs formed as a consequence of its extended evolved nuclear starburst (García-Burillo et al. 2002; Fuente et al. 2006; van der Tak et al. 2008).

Observational evidences point to a significant enhancement in the abundance of HOC⁺ in regions with large ionization fractions. The abundance ratio [HCO⁺]/[HOC⁺]= 270 is found in the prototypical Galactic PDRs of the Orion Bar (Apponi et al. 1999). Similar or even lower abundance ratios are observed in the PDRs NGC 7023 (50-120, Fuente et al. 2003), Sgr B2(OH) and NGC 2024 (360-900, Ziurys & Apponi 1995; Apponi & Ziurys 1997), and the Horsehead (75-200 Goicoechea et al. 2009), as well as in diffuse clouds (70-120, Liszt et al. 2004). This is in contrast with the much larger ratios of $\gg 1000$ found in dense molecular clouds well shielded from the UV radiation. However, these low HCO⁺/HOC⁺ ratios are not found in other galactic PDRs. Large values of this ratio of $\gtrsim 2000$ are found in the PDRs M17-SW, S140, and NGC2023 (Apponi et al. 1999; Savage & Ziurys 2004). The HCO molecule has also been observed to be a particularly good tracer of the PDR interfaces. Low ratios of [HCO⁺]/[HCO] $\sim 2.5 - 30$ are found in prototypical Galactic PDRs (Schenewerk et al. 1988; Schilke et al. 2001). The large HCO abundance ($> 10^{-10}$) altogether with the low ratio [HCO⁺]/[HCO] ~ 1 in the Horsehead PDR is claimed to be a diagnostic for an ongoing FUV-dominated photochemistry (Gerin et al. 2009). CO⁺ is

also claimed to be particularly prominent in the chemical modeling of PDRs and high abundances of this molecule appear to be correlated to similar enhancements of HOC^+ (Sternberg & Dalgarno 1995; Savage & Ziurys 2004). $[\text{CO}^+]/[\text{HOC}^+]$ ratios in the range of 1-10 are observed in a number of PDRs (Savage & Ziurys 2004), but only of $\gtrsim 0.1$. towards the Horsehead PDR (Goicoechea et al. 2009).

As mentioned above, this set of PDR probes has been extensively studied towards M82. However, no such complete studies have been carried out towards other prototypical galaxies, but for the detection of HCO and HOC^+ towards NGC 1068 (Usero et al. 2004) and H_3O^+ in Arp 220 (van der Tak et al. 2008). M82 and NGC 253 are the brightest prototypes of nearby SB galaxies, at a similar distance and showing very similar IR luminosities and star formation rates of about $\sim 3 M_\odot \text{yr}^{-1}$ (Ott et al. 2005; Minh et al. 2007). However, both galaxies show very different chemical composition. The chemistry and to a large extend the heating in the central region of NGC 253 is believed to be dominated by large scale low velocity shocks (Martín et al. 2006b). The similar chemical composition found in the nuclear region of NGC 253 to that in Galactic star forming molecular complexes points to an earlier evolutionary stage of the starburst in this galaxy than that in M82 (Martín et al. 2003, 2005, 2006b).

Furthermore, our recent observations of the PDR component as traced by the easily photodissociated HNCO molecule towards a sample of galaxies (Martín et al. 2008) showed the non-detection of HNCO in M82, at a very low abundance limit. This low HNCO abundance supports the scenario that the PDR chemistry dominates the molecular composition of the ISM in this galaxy. However, from the HNCO measured abundance in NGC 253, it would be placed in an intermediate stage of evolution where photodissociation should be starting to play a significant role in driving a UV-dominated chemistry which has not been yet identified towards this galaxy. The presence of a significant PDR component

in NGC 253 claimed from the HNC/O abundance is also inferred from the similar intensity of the atomic fine structure line intensities from PDR tracers like CII and OI (Carral et al. 1994; Lord et al. 1996) observed in both M 82 and NGC 253.

In this paper we present the first detection of PDR molecular tracers HOC^+ and CO^+ , and confirm the detection HCO (tentatively detected by Sage & Ziurys 1995) in the central region of NGC 253 which allows the evaluation of the influence of the photodissociation radiation in the nuclear ISM of this SB galaxy. The results presented here support the scenario of the presence of a significant PDR component and clearly show the potential of molecular complexity in estimating the contribution of the different heating mechanisms of the ISM in the nuclei of galaxies.

2. Observations and Results

The observations presented in this paper were carried out at the IRAM 30 m and JCMT telescopes on Pico Veleta, Spain, and Mauna Kea, USA, respectively.

2.1. IRAM 30 m

The IRAM 30 m observations were performed in symmetrical wobbler switched mode with a frequency of 0.5 Hz and a beam throw of $4'$ in azimuth. The 516×1 MHz filter banks were used as spectrometers.

We have observed the transitions of C^{18}O $J = 1 - 0$ (109.782 GHz), HCO^+ $J = 1 - 0$ (89.188 GHz), HOC^+ $J = 1 - 0$ (89.487 GHz) and $3 - 2$ (268.451 GHz), and the HCO $1_{0,1} - 0_{0,0}$ (86.670 GHz). Beam sizes at these frequencies were $22''$, $28''$, and $9''$. The nominal position for the observation was $\alpha_{J2000} = 00^{\text{h}}47^{\text{m}}33^{\text{s}}.3$, $\delta_{J2000} = -25^{\circ}17'23''$ for HCO^+ and

HOC⁺, matching up the position used for the 2 mm line survey (Martín et al. 2006b). The data on C¹⁸O and HCO were centered at $\alpha_{J2000} = 00^{\text{h}}47^{\text{m}}33^{\text{s}}.5$, $\delta_{J2000} = -25^{\circ}17'27''$. The two positions are separated by $< 5''$ which, considering the 3 mm beam sizes, should have a negligible influence in the relative intensities. Double Gaussian profiles have been fitted to all observed transitions and the corresponding derived fitting parameters are summarized in Table 1.

Fig. 1 shows the simultaneously observed $J = 1 - 0$ features of HCO⁺ and HOC⁺ compared to the C¹⁸O $J = 1 - 0$ line profile. Although at this frequency the SIS receivers image band rejection is larger than 20 db, we observed the HOC⁺ line tuned to two different velocities (250 and 500 km s⁻¹) in order to confirm that the observed profile was not line emission coming from the upper side band. Fig. 1 shows the average of both observations. The HCO⁺ $J = 1 - 0$ was detected at the edge of the band covered in the 500 km s⁻¹ tuning of HOC⁺. Although pointing accuracy was of the order of 3'', the different shapes observed between the HCO⁺ and HOC⁺ is attributed to a small change in the pointing position during the two observations. This effect accounts for an uncertainty in the integrated intensity of $< 10\%$. Even though the HCO⁺ feature was not completely covered by the backend, the integrated intensity we derive is in agreement within 5% with that of the observed by Nguyen et al. (1992) and we observe the line shape to be consistent with that of C¹⁸O. As indicated in Table 1, only a coarse upper limit to the detection of HOC⁺ $J = 2 - 1$ was obtained.

The HCO $J = 1 - 0$ emission was observed in the same window as SiO $2 - 1$ and H¹³CO⁺ $1 - 0$ and appears slightly blended to the latter. With a significantly improved signal-to-noise ratio, we confirm the previous tentative detection of this HCO transition reported by Sage & Ziurys (1995) with the NRAO 12 m telescope. Moreover, using the main beam brightness temperature from Sage & Ziurys (1995) of ~ 1 mK with at 72'' beam

and our observed ~ 4 mK with a $28''$ beam we can make an estimate of the emitting source extent of $> 20''$. The double Gaussian profiles fitted to each species were constrained to have similar linewidths. The resulting fitted line positions agree within the errors to those expected from the rest frequencies of each line. Fig. 2 shows the results of the fit superimposed on the observations as well as the position of the hyperfine structure lines of HCO. Only the brightest of the group ($F = 2 - 1$) has been taken into account for the fit. Assuming optically thin emission, the $F = 1 - 0$ and $F = 1 - 1$ transitions (at 86.708 and 86.777 GHz) are expected to show an intensity half of the main transition but they are completely blended to the H^{13}CO^+ emission. The $F = 0 - 1$ transition at 86.805 GHz is expected to be even fainter by a factor of 5, well below our detection limit. Fig. 2 shows in dotted line a synthetic spectrum of HCO assuming one velocity component centered at 255km s^{-1} with a linewidth of 192km s^{-1} (as derived if only one component is fitted to the spectrum from the other lines) and a peak intensity of the HCO $F = 2 - 1$ line of 3.6 mK. This shows that the fainter HCO hyperfine transitions may account for up to a 10 – 20% of the H^{13}CO^+ integrated intensity.

2.2. JCMT

JCMT observations were performed in beam switched mode with a frequency of 1 Hz and beam throw of $2'$ in azimuth. The ACSIS digital autocorrelator spectrometer was used with a bandwidth of 1600 MHz providing a resolution of ~ 1 MHz.

We have used the receiver A3 to observe the CO^+ transition at 236.062 GHz. At this frequency, the beam size of the telescope is $21''$ and the main beam efficiency 0.69. The observations were carried towards the nominal position $\alpha_{J2000} = 00^{\text{h}}47^{\text{m}}33^{\text{s}}.1$, $\delta_{J2000} = -25^{\circ}17'18''$ (radio continuum position, Douglas et al. 1996). As seen in the HC_3N $J = 25 - 24$ profile, most of the emission is observed from one of the velocity components

at this position, which is due to the JCMT observed position being $\sim 6''$ and $10''$ away from those observed with the IRAM 30 m, respectively. This position is half beam away from the positions observed with the IRAM 30m, so the abundance ratios derived from this observation might be affected by a larger uncertainty of up to a factor of 2. However, this effect might be attenuated by the emission being extended over scales of $> 20''$.

The $\text{CO}^+ 5/2 - 3/2 F = 2 - 1$ and $3/2 - 1/2 F = 2 - 1$ transitions are clearly detected above the noise level ($\sim 1.5 \text{ mk}$ in 30 km s^{-1} channels). However, we observe its profile significantly blended to that of the group of transitions of $^{13}\text{CH}_3\text{OH } J = 5 - 4$. This overlap was not a problem in the case of the CO^+ detection towards M82 due to the significantly lower abundance of CH_3OH towards this galaxy (Martín et al. 2006a). The $\text{CO}^+ 3/2 - 3/2 F = 2 - 1$ component was not detected due to its low relative intensity. We have fitted the observed profile with a single Gaussian component CO^+ synthetic spectra with radial velocity and linewidth fixed from those derived from HC_3N . The relative intensities of the CO^+ components were also fixed to those expected from optically thin emission under local thermodynamic equilibrium conditions. The derived line profiles parameters are presented in Table 1. Additionally, we simultaneously fitted a synthetic $^{13}\text{CH}_3\text{OH}$ spectra, using the 18 $^{13}\text{CH}_3\text{OH}$ transitions in the observed frequency range, using the same constraints as for the CO^+ line fit. The fit reproduces most of the observed features and shows that the emission from $^{13}\text{CH}_3\text{OH}$ may explain the observed non Gaussian CO^+ profiles. Only the parameters derived for the three most intense components in the group are given in Table 1. This is the first time that the ^{13}C isotopologue of methanol is detected towards an extragalactic source. Regarding the accuracy of the fitted parameters presented in Table 1, the integrated line intensities derived for CO^+ and $^{13}\text{CH}_3\text{OH}$ are likely underestimated by $\sim 20\%$ due to the baseline determination. In the next Section, we discuss the detection of $^{13}\text{CH}_3\text{OH}$ in the context of the derived abundances with respect to those of the main methanol isotopologue.

3. Molecular abundances and ratios

We have estimated the fractional abundances of the newly observed species in NGC 253 assuming optically thin emission, LTE conditions, and similar spatial distribution for all species. Under these assumptions, we have calculated the column densities of H^{13}CO^+ , HOC^+ , HCO , and CO^+ for an excitation temperature $T_{\text{ex}} = 15 \pm 5 \text{ K}$ and an estimated source extent for each velocity component of $10''$. The $T_{\text{ex}} = 15 \pm 5 \text{ K}$ is assumed based on the average rotational temperatures derived from most of the species detected towards NGC 253 (Martín et al. 2006b). Indeed the non detection of $\text{HOC}^+ 3 - 2$ implies low excitation temperatures of $T_{\text{ex}} \sim 10 \text{ K}$. Both the excitation temperature and the emission extent have an important impact in the absolute derived column densities by up to a factor of 2, however, the fractional abundances and abundance ratios are mostly independent of these assumptions. We assume that the emission extent is similar for all observed species. Table 2 presents the column densities and fractional abundance ratios with respect to H_2 for all the species. The total H_2 column density has been derived from the C^{18}O column density for each velocity component assuming an isotopic ratio of $^{16}\text{O}/^{18}\text{O} = 150$ (Harrison et al. 1999) and a $\text{CO}/\text{H}_2 = 10^{-4}$. The relative abundances derived for all molecules are presented in Table 2. Additionally, abundance ratio of H^{13}CO^+ with respect all species is also presented in Table 2. The errors in the derived column densities take into account the statistical error of integrated intensities and the uncertainty in the assumed excitation temperature. These errors are subsequently propagated to the abundance ratios. The HCO^+ abundance has been derived from that of H^{13}CO^+ to avoid the opacity effects affecting the main isotopologue. Indeed, if the $^{12}\text{C}/^{13}\text{C}$ ratio of ~ 40 derived for NGC 253 and NGC 4945 (Henkel et al. 1993, 1994; Martín et al. 2005) applies to all these galaxies, an average opacity of $\tau_{\text{HCO}^+ J=1-0} \gtrsim 1$ is derived from the $\text{HCO}^+/\text{H}^{13}\text{CO}^+ J = 1 - 0$ line ratio (this work and Usero et al. 2004). As a consequence, ratios may be underestimated by a factor of ~ 2 if derived from the main isotopologue. The CO^+ column density presents

a significant uncertainty due to its blending with the newly detected isotopologue of methanol, $^{13}\text{CH}_3\text{OH}$. However, the CO^+ abundance should not be affected by more than a factor of 2.

We have derived a column density for $^{13}\text{CH}_3\text{OH}$ of $\sim 1.6(1.0) \times 10^{14} \text{ cm}^{-2}$. If we compare this column density with that of the main isotopologue from (Martín et al. 2006b) it results in a $\text{CH}_3\text{OH}/^{13}\text{CH}_3\text{OH}$ ratio of 12 ± 7 , significantly lower than the ratio $^{12}\text{C}/^{13}\text{C}=40$ (Henkel et al. 1993). Both the difference of $6''$ in the observed positions and a different filling factor of CH_3OH might account for part of this difference. However, the integrated intensities measured for the methanol group of transitions at 145.1 GHz by Martín et al. (2006b) and Hüttemeister et al. (1997) at positions differing by $> 13''$ show a variation of $< 6\%$ so the difference in positions is not likely to contribute to this difference. Thus, opacity is likely the dominant effect as observed in the Galactic center (GC, Requena-Torres et al. 2006). From the $^{12}\text{C}/^{13}\text{C}$ ratio in NGC 253 we derive a fractional abundance of methanol of $\sim 10^{-7}$, close to the abundances observed in the Galactic center (Requena-Torres et al. 2006). Methanol is, after CO and NO, the most abundant molecule in the nucleus of NGC 253 (Martín et al. 2006b).

4. Discussion: The PDR component in NGC 253

4.1. NGC 253 in context

Table 3 shows the $\text{HCO}^+/\text{HOC}^+$, HCO^+/HCO , and HCO^+/CO^+ abundance ratios resulting from our measurements in NGC 253 compared to those of the similar SB galaxy M 82, and the Seyfert 2 with nuclear SBs, NGC 1068, and NGC 4945, together with prototypical galactic PDRs, where observations of these species have been reported. For the sake of consistency, the abundance ratios of the other galaxies have been calculated

from the available line profiles obtained from the literature. As already explained before, for this comparison we used H^{13}CO^+ to derive the HCO^+ column densities in order to avoid the opacity effects. We have assumed the isotopic ratio of $^{12}\text{C}/^{13}\text{C}=40$ (Henkel et al. 1993) to derive the column densities of the main isotopologue. For M 82, the $\text{HCO}^+/\text{HOC}^+$ and HCO^+/CO^+ abundance ratio have been derived from the observations by Fuente et al. (2006) towards the Eastern molecular lobe. Our measured ratios are ~ 59 and ~ 0.8 , which are $> 30\%$ larger than the ratios derived by Fuente et al. (2006). This difference is due to the significant missing flux of the H^{13}CO^+ interferometric maps (García-Burillo et al. 2002) they used for comparison, as well the higher $^{12}\text{C}/^{13}\text{C}$ ratio they used to compare with single dish HCO^+ observations. By comparing the convolved integrated intensity from the H^{13}CO^+ interferometric maps by (García-Burillo et al. 2002) towards the western lobe Fuente et al. (2006) and the single dish data of by Mauersberger & Henkel (1991) towards a nearby position, we have estimated a $\gtrsim 50\%$ missing flux. Thus we used the $\text{H}^{13}\text{CO}^+ 1 - 0$ data by Mauersberger & Henkel (1991) in our measured ratios. The ratios towards NGC 1068 were derived for the regions within the galaxy where lines intensities were tabulated by Usero et al. (2004). The observations from Wang et al. (2004) were used to derive the HCO^+/HCO ratio towards NGC 4945.

4.1.1. PDR abundance ratios in SB galaxies

We find that the three derived $\text{HCO}^+/\text{HOC}^+$, HCO^+/HCO , and HCO^+/CO^+ abundance ratios in the two starbursts, NGC 253 and M 82, are equivalent within the measurement errors. The ratios are also in reasonable good agreement to those found in galactic sources with similar FUV fluxes (see Table 3). Such high abundances ratios of HOC^+ , HCO , and CO^+ relative to HCO^+ have been claimed to be the evidence of M 82 being mostly dominated by photodissociation. We notice that the average HCO^+/HCO

ratio in NGC 253 are even lower than that measured in M 82. In the case of HCO, the interferometric maps of M 82 clearly resolve the spatial variations in this ratio across the galaxy nuclear region. However, towards the region of peak HCO emission in the M 82 maps, we find a ratio of $\text{H}^{13}\text{CO}^+/\text{HCO} \sim 0.12 \pm 0.04$, equivalent to the average observed towards NGC 253. Our data show that the ISM in the nuclear region in NGC 253 must be significantly pervaded by a strong UV radiation flux from the massive star clusters formed in the starburst, as also suggested by the study of the abundances of the HNC/CS ratio (Martín et al. 2009). Moreover, these new observations would imply that photodissociation plays a similar role in the ISM heating of both NGC 253 and M 82.

4.1.2. *PDR abundance ratios in AGN galaxies*

Both HCO^+/HCO and $\text{HCO}^+/\text{HOC}^+$ abundance ratios in NGC 1068 are different by a factor 2 – 3 from those of NGC 253 and M 82. Furthermore, HCO^+/HCO is also found to be up to a factor of ~ 2 lower in the ring of star formation than towards the nuclear region. Like in NGC 253, these ratios are consistent with the decrease in the abundance of molecules such as HNC from the nuclear region to the starburst ring (Martín et al. 2009). The tentative detection of HCO in the circunuclear disk (CND) of NGC 1068 (Usero et al. 2004), suggest a rough H^{13}CO^+ to HCO line intensity ratio of $\sim 2 - 3$, which turns into an abundance ratio in the range of $\sim 0.09 - 0.13$, closer to the values derived in SB dominated galaxies. This value at the CND can be significantly biased by the emission from the star forming ring covered at half-power by the $28''$ beam. Therefore, it is clear that this ratio does not significantly decrease towards the nuclear AGN in this galaxy with the typical angular resolution of $20'' - 30''$. On the other hand, the ratio $\text{HCO}^+/\text{HOC}^+$ is only a factor of 2 lower in the starbursts galaxies than towards the nuclear AGN in NGC 1068. From these observations, it is unclear whether photodissociation does play a major role in the

AGN dominated center of NGC 1068. Unfortunately, no observations of HOC^+ are available towards the SF ring in this galaxy.

Similar to NGC 1068, the obscured Seyfert 2 nucleus in NGC 4945 is surrounded by a starburst ring more prominent than in NGC 1068 (Genzel et al. 1998). The HCO^+/HCO ratio found in NGC 4945 is even lower than that found in the other galaxies. However, the fit to these lines was claimed to be very uncertain by Wang et al. (2004).

4.2. Comparison to PDR chemical models

We have compared our observed fractional abundances and abundance ratios with those predicted by the UCL_PDR model (Bell et al. 2006). The UCL_PDR code is a time and depth dependent one dimensional PDR model that simultaneously solve the chemistry, thermal balance and radiative transfer within a cloud (see Bell et al. 2006, for more details). We have adopted a hydrogen density of 10^5 cm^{-3} , a radiation field $G_0 \sim 5000$ in units of Habing field, and a cosmic radiation rate of 10^{-16} . The high density of 10^5 cm^{-3} is derived from the multiline analysis of CS and HC_3N (Bayet et al. 2008, 2009, ; Aladro et al. In Prep). Our estimates of the cloud structure (see Sect. 4.3) depends on the averaged radiation field which might be different in both galaxies. The averaged radiation fields in both NGC 253 and M 82 have been inferred from the fine structure lines and they are of 2×10^4 and 10^3 , respectively, with large errors of a factor of 2 (Carral et al. 1994; Lord et al. 1996). This would imply that the PDR envelope should be larger in the clouds of NGC 253 than in M 82. Since we do not aim to quantitatively model the particular abundances measured in NGC 253 but to investigate the physical conditions that would give rise to the wealth of observed molecules in starburst, the value of $G_0 = 5 \times 10^3$ used is a geometric mean value derived from the fine structure lines in both galaxies. Given that our estimates of the A_v for the PDR are based on this geometric mean, the expected changes in A_v for

the two galaxies would be just a factor of 1.6.

We have ran two different models: Model A is a standard time dependent gas-phase PDR model where the initial composition is atomic; while Model B is computed using a coupled dense core-PDR model where the diffuse material, initially also purely atomic and gaseous, collapses to reach a final density of 10^5 cm^{-3} . During the collapse the gas depletes on the grains forming icy mantles which remain on the dust until irradiation from a UV field is switched on, evaporation occurs and the typical PDR chemistry takes place. In both models the temperature is calculated self-consistently at each depth and time step by thermal balance. Fig. 4 shows the predicted abundances and abundance ratios as a function of visual extinction (A_v) for Model A (left panels) and B (right panels). HNC and CH_3OH results are only shown for Model B in Fig. 4.

Observed abundances of HCO^+ and HOC^+ towards NGC 253 (shown as horizontal lines in the key of Fig. 4) are well reproduced by the models for very low extinction of $A_v \sim 1 - 2$. The HCO abundance observed is a factor 2 – 6 above the maximum predicted by the model B. It is important to take into account that while we assumed a ratio $\text{CO}/\text{H}_2=10^{-4}$ to calculate the fractional abundances, this ratio is not constant in the models and hardly ever reaches this value. On the other hand, the abundance ratios of the observed molecules, unaffected by the hydrogen determination uncertainty, agree well with the model predictions. The model shows that the abundances of CO^+ , follows the same pattern as HOC^+ . The correlation between these two molecules was also predicted by previous theoretical studies (Sternberg & Dalgarno 1995; Savage & Ziurys 2004). Thus, CO^+ measurement allows us to confirm the effect of photodissociation suggested by the large abundance of HOC^+ .

The ions HOC^+ , CO^+ and HOC^+ are mostly formed at the edge of the cloud and while the two models predict similar abundances for these ions, it is worth noting that

the observed abundances of other species such as HNCO, CH₃OH, or HOCO⁺ can only be explained with Model B. However, HNCO and CH₃OH only reach observable abundances for $A_v \sim 5$ magnitudes. This implies that, while photodissociation does play an important role in the chemistry of NGC253, the molecular clouds affected by the UV radiation must contain a dense core well shielded from the UV radiation and rich with gas phase icy mantle molecules like HNCO and CH₃OH.

4.3. The molecular clouds in SB galaxies

Martín et al. (2008) have used a comparison with the GC molecular clouds to propose another PDR diagnostic based on the relative abundance of HNCO to CS. The large variation of the HNCO/CS abundance ratio between UV radiated clouds to those well shielded clouds only affected by shocks was interpreted as the fast photodissociation of the fragile molecule HNCO, efficiently produced on the icy mantles and delivered into gas phase by low velocity shocks. Similarly, in a sample of nearby galaxies Martín et al. (2009) found changes of nearly two orders of magnitude from the shock dominated chemistry in M 83 and IC 342 to UV dominated chemistry in M 82. The extremely low HNCO abundance in M 82 and the large abundances of HCO, HOC⁺ and CO⁺ support the idea that the HNCO/CS ratio is a measure of the relative importance of the UV heating to shock heating and the evolutionary state of the starburst in galaxies.

The detection of HCO, HOC⁺ and CO⁺ in NGC253 with similar column densities and abundance to those in M82 suggest that the PDR component is similar in both galaxies as suggested by the similar atomic fine structure line intensities in both galaxies. The results of model B confirm the observational trends observed in HNCO and the other PDR molecules in galaxies. For molecular clouds with $A_v \sim 1 - 2$ (i.e column densities of $1 - 2 \times 10^{21} \text{cm}^{-2}$) illuminated by a strong UV radiation field like in the galaxies in

our sample, HNC and CH₃OH are largely photodissociated and only HCO, HOC⁺ and CO⁺ should be observed like in M82 (Martín et al. 2006a, 2009). Then, not very massive molecular clouds and widely translucent to the UV radiation should dominate in M82. On the other hand, for galaxies with massive molecular clouds (large visual extinction) or low UV radiation fields, HNC and CH₃OH are well shielded and the abundance ratio of HNC/CS will reach its maximum value. Considering that M83 and IC342 represent the stage of galaxies with an extremely low PDR component, the lower HNC/CS ratios measured for NGC253, NGC4945 and NGC1068 indicate that the PDR component must be substantial, as observed in other PDR tracers.

For NGC253 we find that the PDR component is similar to that in M82, but the total column density of dense gas is a factor of 2-3 larger in NGC253 than in M82 from the low HNC and CH₃OH abundance in the latter. Considering the PDR column densities in both galaxies are similar, this component should represent about 1/3 – 1/2 of the total molecular column density in NGC253. This is roughly consistent with the decrease by a factor of 2 – 3 of the HNC/CS ratio as compared with that of M83 or IC342 (Martín et al. 2009). This suggests that the molecular clouds properties in M82 and NGC253 must be quite different in terms of the total molecular column density, which implies that the sizes or the densities are different, or a combination of both. Using the atomic fine structure and CO emission lines, Carral et al. (1994) and Lord et al. (1996) have also proposed that the clouds in M82 and NGC253 are quite different. The clouds in NGC253 are slightly smaller than those in M82, but with masses a factor of 15 larger than for M82. The NGC253 average cloud column densities are therefore factor of 20 larger than in M82. Though the total column densities of the M82 clouds inferred from the atomic fine structure lines are a factor of 5 larger than those predicted from the PDRs tracers and the HNC abundance in this galaxy, similar constrains are derived both the molecular and the atomic tracers. Therefore, the clouds in NGC253 are more massive than in M82.

We can even make a very rough estimate of the average properties and structure of the molecular clouds in NGC 253 and M 82 by combining the complementary information obtained from the PDR tracers presented in this paper and the HNC0 column densities from (Martín et al. 2009). While HCO, HOC⁺ and CO⁺ mainly trace the PDR region up to $A_v = 4 - 5$ (i.e. H₂ column densities of $5 \times 10^{21} \text{cm}^{-2}$), the HNC0 emission only arises from the well shielded core ($A_v > 7$) of the molecular clouds. The HCO, HOC⁺ and CO⁺ column densities in NGC 253 and M 82 indicate similar averaged column densities in the PDR envelopes of the molecular clouds in both galaxies. The big difference in the molecular cloud structure in both galaxies is in the size (H₂ column density) of the well shielded cores of the molecular clouds. In the case of M 82, where HNC0 has not been detected, we can set an upper limit to the HNC0 column density of $7 \times 10^{12} \text{cm}^{-2}$. This translates to a upper limit to the core H₂ column density of $< 3 \times 10^{20} \text{cm}^{-2}$ for the HNC0 fractional abundance of 2×10^{-8} derived for the well shielded clouds in the galactic center (Martín et al. 2008). The averaged shielded cloud cores in M 82 are smaller by more than one order of magnitude than the PDR envelope. In the case of NGC 253, the H₂ column densities of the shielded cloud cores is 10^{22}cm^{-2} , a factor of 2 larger than PDR envelope. Assuming a similar averaged density distribution in the molecular clouds in both galaxies, the clouds in NGC 253 would be a factor 2 – 3 larger than in M 82.

4.4. The contribution X-ray induced chemistry

The PDR model presented by Fuente et al. (2006) failed to reproduce the large CO⁺ column density of a few 10^{13}cm^{-3} observed towards M 82. This lead Spaans & Meijerink (2007) to explore the possibility of an enhanced X-ray induced chemistry in this galaxy. Spaans & Meijerink (2007) concluded that such high formation of CO⁺ can only be explained by X-ray irradiated molecular gas with densities of $10^3 - 10^5 \text{cm}^{-3}$. Although the

X-ray luminosity of NGC 253 is a factor of 2 – 4 below that of M 82, both galaxies have a significant X-ray emission in the range of $\sim 10^{40}$ erg s $^{-1}$ (Cappi et al. 1999). Similar to M 82, the NGC 253 total CO $^+$ column density is $(3.6 \pm 1.1) \times 10^{13}$ cm $^{-2}$. Moreover, both show a similar HCO $^+$ /CO $^+$ ratio of $\sim 30 - 40$.

The models presented in this paper are able to produce such column densities for visual extinctions of $A_v \sim 3-5$ for model A, and $A_v \sim 0.5-1$ for model B. These models have been calculated with a radiation field, a cosmic ray flux and a H $_2$ density smaller by a factor of 2, 40 and 4, respectively, with respect to those assumed in the models of Fuente et al. (2006). Furthermore, we are able to reproduce the abundances and abundance ratios measured for all the other observed species presented in this paper. van der Tak et al. (2008) showed how the measured abundance of H $_3$ O $^+$ in M 82 can be both produced by PDR with a high cosmic-ray ionization or by an XDR. Indeed, an increase of cosmic ray ionization rate in PDR models may be qualitatively used to simulate XDR-like environments. Our models, however, do not use particularly high cosmic ray fluxes (a factor of 5 higher than standard). Thus, though the X-ray irradiation is substantial in SB galaxies, the PDR models presented in this paper can reproduce the molecular abundances observed towards the brightest prototypes, M 82 and NGC 253. Moreover, no significant changes in the abundances of HOC $^+$ and HCO are found towards the nuclear AGN of NGC 1068 where X-ray radiation is significantly more important than in SB nuclei, as shown in Sect. 4.1.2. Unfortunately, no CO $^+$ observation has been reported towards this Seyfert 2 nucleus.

5. Conclusions: The pervading UV field in evolved starburst

The comparison of model predictions with the observations presented show that the abundance of the species observed in this work towards NGC 253, namely HCO $^+$, CO $^+$, and HCO, are most efficiently formed in the outer region of the molecular clouds

where the gas is highly irradiated by the incident UV photons from massive stars. The high molecular abundances derived for these species in NGC 253 suggest that the PDR component in this galaxy is similar to that found in M 82, claimed to be the prototype of extragalactic PDR. The abundance ratios found for this limited sample of galaxies are of the same order as those observed towards galactic PDRs, which stress the importance of photo-dominated chemistry in galaxy nuclei. Large amounts of molecular material are affected by photodissociation not only in NGC 253, but also towards the star forming regions around the Seyfert 2 nuclei in NGC 4945 and NGC 1068. This is consistent with the HNC/CO ratio in these galaxies which suggest that a fraction of HNC has been photodissociated in PDRs. The combination of the observations of HCO, HOC⁺ and CO⁺ with that of HNC seems to confirm that their abundances reflect the evolutionary stage of the starbursts in these galaxies. Although photodissociation is the most likely scenario for the enhancement of the observed reactive ion in starburst environments, X-ray dominated chemistry has been claimed to be responsible for the high abundances observed around AGNs in circunuclear disk of NGC 1068 (HOC⁺ Usero et al. 2004) and towards the ultra luminous infrared galaxy Arp 220 (H₃O⁺ van der Tak et al. 2008).

Therefore, M 82 is still outstanding not only as a PDR dominated galaxy, but by the underabundance of complex molecules such as CH₃OH, HNC or SiO (Mauersberger & Henkel 1993; Martín et al. 2006a,b), evidence for the lack of large amounts of dense molecular material which would potentially fuel its nuclear starburst as compared to other starburst galaxies like NGC 253 (Martín et al. 2009). Our data in combination with the HNC abundances (Martín et al. 2009) indicate that the molecular clouds in M 82 are different from those in NGC 253. Although having a similar overall PDR component, the clouds in NGC 253 have to be more massive and have larger column densities those in M 82.

This work has been partially supported by the Spanish Ministerio de Ciencia e Innovación under project ESP2007-65812-C02-01, and by the “Comunidad de Madrid” Government under PRICIT project S-0505/ESP-0237 (ASTROCAM).

Facilities: IRAM 30m, JCMT.

REFERENCES

- Apponi, A. J., & Ziurys, L. M. 1997, *ApJ*, 481, 800
- Apponi, A. J., Pesch, T. C., & Ziurys, L. M. 1999, *ApJ*, 519, L89
- Bayet, E., Lintott, C., Viti, S., Martín-Pintado, J., Martín, S., Williams, D. A., & Rawlings, J. M. C. 2008, *ApJ*, 685, L35
- Bayet, E., Aladro, R., Martín, S., Viti, S., Martín-Pintado, J. 2009, Submitted to *ApJ*
- Bell, T. A., Roueff, E., Viti, S., & Williams, D. A. 2006, *MNRAS*, 371, 1865
- Cappi, M., et al. 1999, *A&A*, 350, 777
- Carral, P., Hollenbach, D. J., Lord, S. D., Colgan, S. W. J., Haas, M. R., Rubin, R. H., & Erickson, E. F. 1994, *ApJ*, 423, 223
- Douglas, J. N., Bash, F. N., Bozayan, F. A., Torrence, G. W., & Wolfe, C. 1996, *AJ*, 111, 1945
- Fuente, A., Rodríguez-Franco, A., García-Burillo, S., Martín-Pintado, J., & Black, J. H. 2003, *A&A*, 406, 899
- Fuente, A., García-Burillo, S., Gerin, M., Rizzo, J. R., Usero, A., Teyssier, D., Roueff, E., & Le Bourlot, J. 2006, *ApJ*, 641, L105
- García-Burillo, S., Martín-Pintado, J., Fuente, A., & Neri, R. 2000, *A&A*, 355, 499
- García-Burillo, S., Martín-Pintado, J., Fuente, A., Usero, A., & Neri, R. 2002, *ApJ*, 575, L55
- Genzel, R., et al. 1998, *ApJ*, 498, 579
- Gerin, M., Goicoechea, J. R., Pety, J., & Hily-Blant, P. 2009, *A&A*, 494, 977

- Goicoechea, J. R., Pety, J., Gerin, M., Hily-Blant, P., & Le Bourlot, J. 2009, *A&A*, 498, 771
- Harrison, A., Henkel, C., & Russell, A. 1999, *MNRAS*, 303, 157
- Henkel, C., Mauersberger, R., Wiklind, T., Hüttemeister, S., Lemme, C., & Millar, T. J. 1993, *A&A*, 268, L17
- Henkel, C., Whiteoak, J. B., & Mauersberger, R. 1994, *A&A*, 284, 17
- Hüttemeister, S., Mauersberger, R., & Henkel, C. 1997, *A&A*, 326, 59
- Liszt, H., Lucas, R., & Black, J. H. 2004, *A&A*, 428, 117
- Lord, S. D., Hollenbach, D. J., Haas, M. R., Rubin, R. H., Colgan, S. W. J., & Erickson, E. F. 1996, *ApJ*, 465, 703
- Martín, S., Mauersberger, R., Martín-Pintado, J., García-Burillo, S., & Henkel, C. 2003, *A&A*, 411, L465
- Martín, S., Martín-Pintado, J., Mauersberger, R., Henkel, C., & García-Burillo, S. 2005, *ApJ*, 620, 210
- Martín, S., Martín-Pintado, J., & Mauersberger, R. 2006a, *A&A*, 450, L13
- Martín, S., Mauersberger, R., Martín-Pintado, J., Henkel, C., & García-Burillo, S. 2006b, *ApJS*, 164, 450
- Martín, S., Requena-Torres, M. A., Martín-Pintado, J., & Mauersberger, R. 2008, *ApJ*, 678, 245
- Martín, S., Martín-Pintado, J., & Mauersberger, R. 2009, *ApJ*, 694, 610
- Mauersberger, R., & Henkel, C. 1991, *A&A*, 245, 457
- Mauersberger, R., & Henkel, C. 1993, *Reviews in Modern Astronomy*, 6, 69

- Minh, Y. C., Muller, S., Liu, S.-Y., & Yoon, T. S. 2007, *ApJ*, 661, L135
- Nguyen, Q.-R., Jackson, J. M., Henkel, C., Truong, B., & Mauersberger, R. 1992, *ApJ*, 399, 521
- Ott, J., Weiss, A., Henkel, C., & Walter, F. 2005, *ApJ*, 629, 767
- Requena-Torres, M. A., Martín-Pintado, J., Rodríguez-Franco, A., Martín, S., Rodríguez-Fernández, N. J., & de Vicente, P. 2006, *A&A*, 455, 971
- Savage, C., & Ziurys, L. M. 2004, *ApJ*, 616, 966
- Sage, L. J., & Ziurys, L. M. 1995, *ApJ*, 447, 625
- Schenewerk, M. S., Jewell, P. R., Snyder, L. E., Hollis, J. M., & Ziurys, L. M. 1988, *ApJ*, 328, 785
- Schilke, P., Pineau des Forêts, G., Walmsley, C. M., & Martín-Pintado, J. 2001, *A&A*, 372, 291
- Spaans, M., & Meijerink, R. 2007, *ApJ*, 664, L23
- Sternberg, A., & Dalgarno, A. 1995, *ApJS*, 99, 565
- Störzer, H., Stutzki, J., & Sternberg, A. 1995, *A&A*, 296, L9
- Usero, A., García-Burillo, S., Fuente, A., Martín-Pintado, J., & Rodríguez-Fernández, N. J. 2004, *A&A*, 419, 897
- van der Tak, F. F. S., Aalto, S., & Meijerink, R. 2008, *A&A*, 477, L5
- Wang, M., Henkel, C., Chin, Y.-N., Whiteoak, J. B., Hunt Cunningham, M., Mauersberger, R., & Muders, D. 2004, *A&A*, 422, 883
- Ziurys, L. M., & Apponi, A. J. 1995, *ApJ*, 455, L73

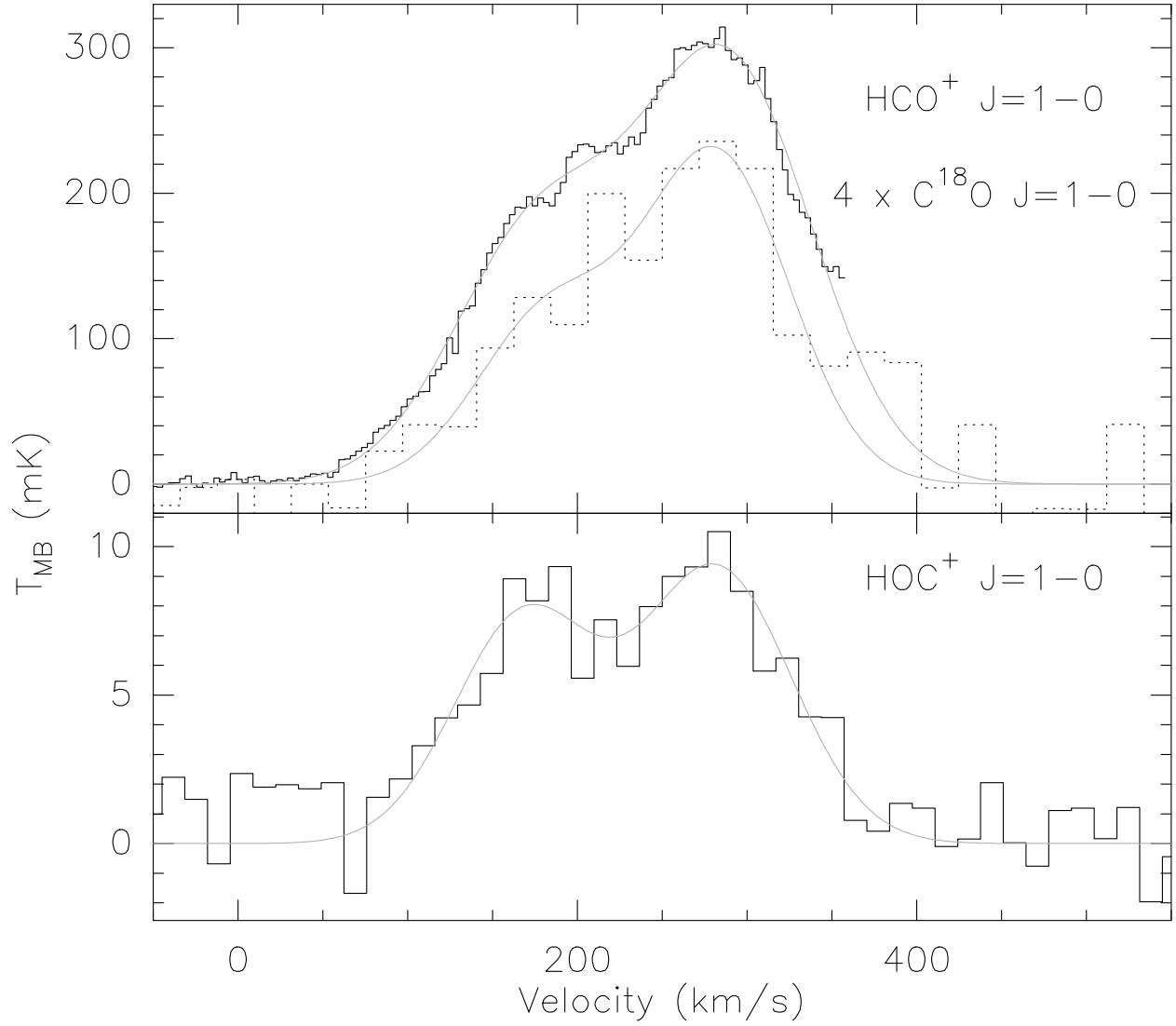


Fig. 1.— IRAM 30 m observations of the emission of HCO^+ , C^{18}O and $\text{HOC}^+ J = 1 - 0$ transitions with the fitted line profiles superimposed. C^{18}O emission has been multiplied by a factor of 4 for comparison with the HCO^+ profile. The spectral resolution are the original 1 MHz ($\sim 3 \text{ km s}^{-1}$) and smoothed to 4 MHz ($\sim 13 \text{ km s}^{-1}$), respectively.

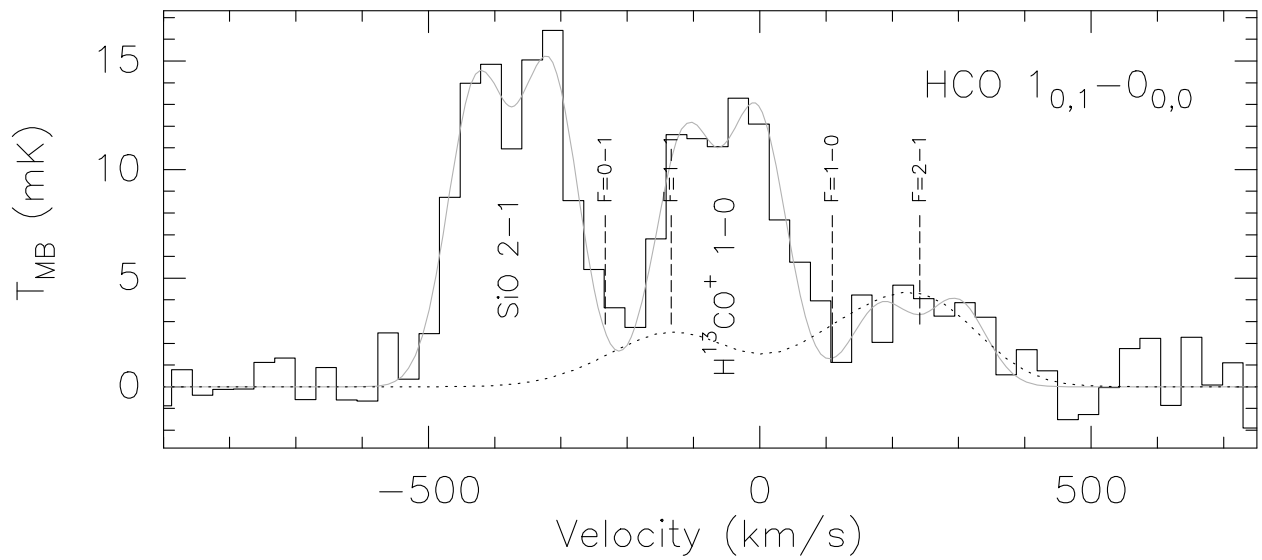


Fig. 2.— HCO profile in the same window as SiO and H^{13}CO^+ observed with the IRAM 30 m.. On top it is shown the triple Gaussian profile fitted to the transitions. Dashed lines indicate the position of each hyperfine structure transition of HCO, where only the brighter one has been fitted. The theoretical synthetic spectrum of HCO is shown with a dotted line (see Sect. 2 for details). Velocity resolution has been degraded to $\sim 31 \text{ km s}^{-1}$.

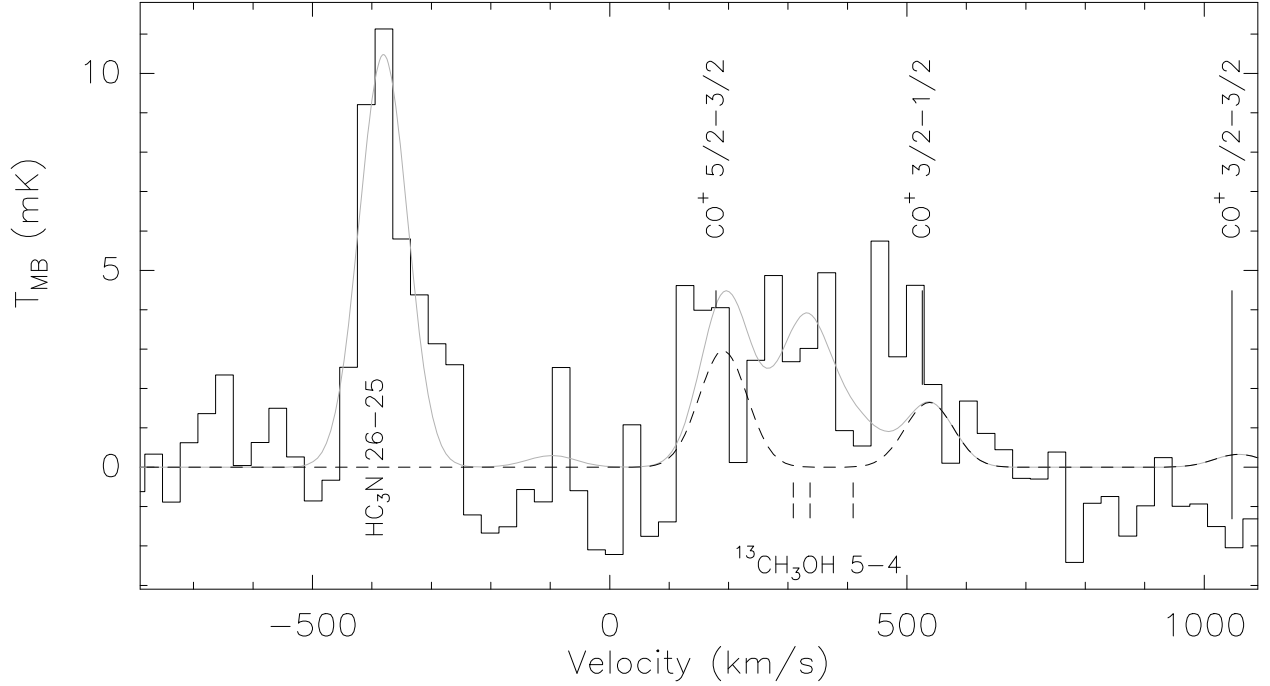


Fig. 3.— JCMT observations of the CO^+ emission blended with transitions of $^{13}\text{CH}_3\text{OH } J = 5 - 4$ and observed in the same window as $\text{HC}_3\text{N } J = 25 - 24$. This is the first detection of the ^{13}C isotopologue of methanol. The overall spectral fitting to all the lines is shown in grey. The contribution of the CO^+ emission is shown with dashed line. The position of the three brighter transitions of the $J = 5 - 4$ group of $^{13}\text{CH}_3\text{OH}$ are shown indicated with vertical dashed lines. See Sect. 2 for details on the fitting to the spectra. Velocity resolution has been degraded to $\sim 30 \text{ km s}^{-1}$.

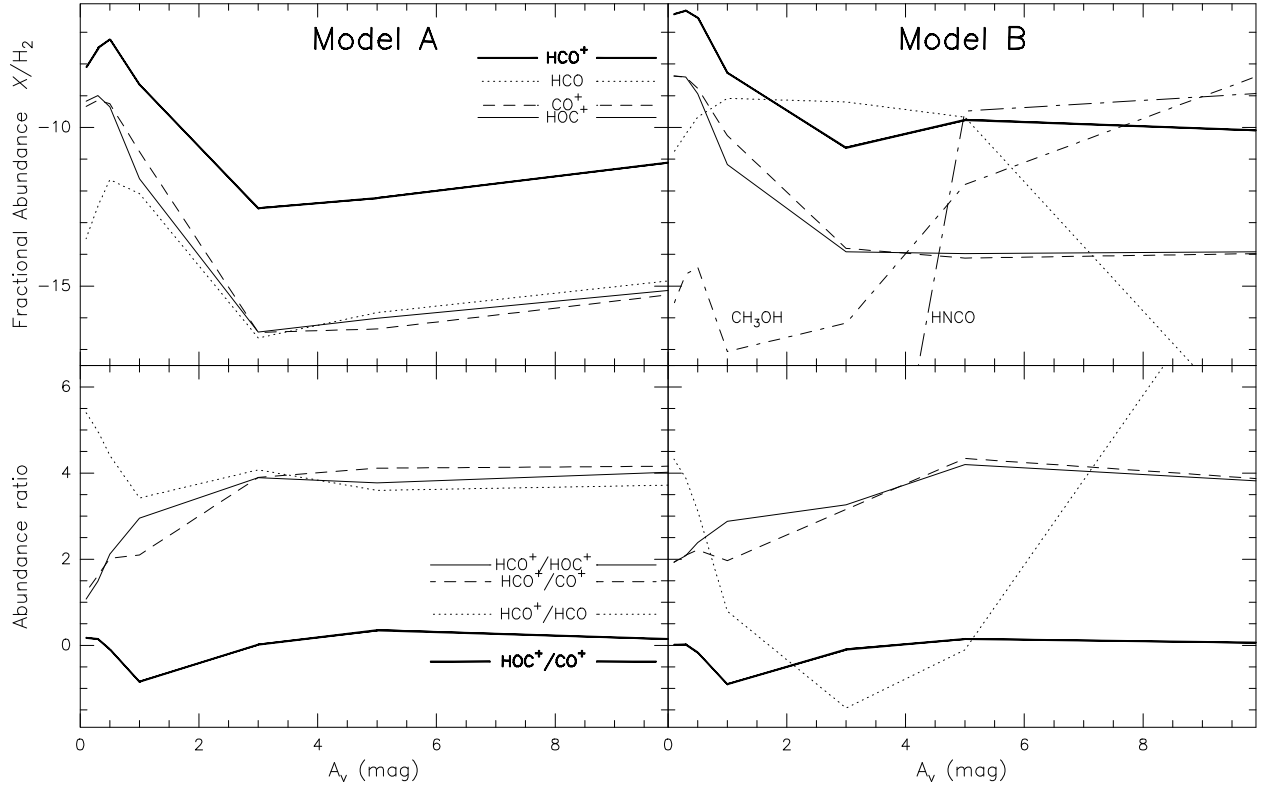


Fig. 4.— Theoretical predictions for the fractional abundances relative to H_2 (*Upper panels*) and abundance ratios (*Lower Panels*) for the observed species as derived from the two different PDR models: a pure gas-phase model A (*Left panels*) and a coupled dense core-PDR model B (*Right panels*). Details are given in Section 4.2. The vertical position of the key for each molecule and ratio shown only in the plots for model A correspond to the actual derived parameters from the observations. Additionally, the fractional abundances of CH_3OH and $HNCO$ are shown for model B.

Table 1: Parameters derived from the observed line profiles.

Transition	$\int T_{\text{MB}} dv$ (K km s ⁻¹)	v_{LSR} (km s ⁻¹)	$\Delta v_{1/2}$ (km s ⁻¹)	T_{MB} (mK)
C ¹⁸ O 1 – 0	3.1 ± 0.6	183 ± 13	100 ± 9	116.75
	6.0 ± 0.8	283 ± 7	100 ± 9 ^a	223.48
HCO ⁺ 1 – 0	21.98 ± 1.1	177.9 ± 0.4	118.1 ± 0.3	174.9
	35.79 ± 1.4	289.0 ± 0.3	118.1 ± 0.3 ^a	284.8
HOC ⁺ 1 – 0	0.8 ± 0.2	170 ± 10	100 ± 20	7.6
	1.0 ± 0.2	282 ± 9	100 ± 20	9.2
HOC ⁺ 3 – 2	< 0.8 ^b			< 4.1
HCO 1 _{0,1} – 0 _{0,0}	0.41 ± 0.08	183 ± 14	102 ± 4 ^a	3.8
	0.43 ± 0.08	297 ± 13	102 ± 4 ^a	3.9
H ¹³ CO ⁺ 1 – 0	1.26 ± 0.09	176 ± 6	102 ± 4 ^a	11.6
	1.36 ± 0.10	285 ± 5	102 ± 4 ^a	12.5
SiO 2 – 1	1.52 ± 0.11	182 ± 5	102 ± 4 ^a	13.9
	1.59 ± 0.11	292 ± 5	102 ± 4 ^a	14.6
HC ₃ N $J = 5 - 4$	1.05 ± 0.15	191 ± 7	95 ± 18	10.5
CO ⁺ 5/2 – 3/2 $F = 2 - 1$	0.30 ± 0.10	191 ^c	95 ^c	3.0
CO ⁺ 3/2 – 1/2 $F = 2 - 1$	0.17 ± 0.10	191 ^c	95 ^c	1.6
¹³ CH ₃ OH 5 _{0,5} – 4 _{0,4}	0.10 ± 0.07	191 ^c	95 ^c	1.0
¹³ CH ₃ OH 5 _{-1,5} – 4 _{-1,4}	0.16 ± 0.07	191 ^c	95 ^c	1.6

^a Linewidths forced to have the same value in the Gaussian fit.

^b 3 σ upper limit assuming a 200 km s⁻¹ linewidth.

^c Parameters forced to equal those derived from HC₃N Gaussian fit.

Table 2: Derived fractional abundances and H^{13}CO^+ ratios for each velocity component

Molecule	N ($\times 10^{13} \text{ cm}^{-2}$)	$[X]/[\text{H}_2]^a$ (10^{-10})	$\text{H}^{13}\text{CO}^+/X$
H^{13}CO^+	1.6 ± 0.5	4.8 ± 1.0	1
	1.7 ± 0.6	2.7 ± 0.4	1
HOC^+	0.8 ± 0.3	2.4 ± 0.7	2.0 ± 0.8
	1.1 ± 0.4	1.7 ± 0.4	1.6 ± 0.4
HCO	12.3 ± 5.8	37 ± 10	0.13 ± 0.04
	12.9 ± 6.1	20 ± 4	0.14 ± 0.03
CO^+	1.7 ± 0.8	5 ± 2	0.9 ± 0.4

^aWith $N(\text{H}_2) = 3.3 \pm 1.2 \times 10^{22} \text{ cm}^{-2}$ and $6.3 \pm 2.1 \times 10^{22} \text{ cm}^{-2}$ for each velocity component, respectively, as derived from C^{18}O with $^{16}\text{O}/^{18}\text{O} = 150$ (Harrison et al. 1999) and a $\text{CO}/\text{H}_2 = 10^{-4}$.

Table 3: Abundance ratios of HCO⁺ vs HOC⁺ and HCO.

Source	[HCO ⁺]/[HOC ⁺]	[HCO ⁺]/[HCO]	[HCO ⁺]/[CO ⁺]
NGC 253	80 ± 30	5.2 ± 1.8	38 ± 15
	63 ± 17	5.4 ± 1.3	...
M 82	60 ± 28 ^a	9.6 ± 2.8 ^b	32 ± 16 ^a
NGC 1068	128 ± 28 ^c	3.2 ± 1.2 ^d	...
NGC 4945	...	2.4 ± 1.2 ^e	...
<i>GC prototypical PDRs</i>			
Horsehead	75 – 200 ^f	1.1 ^g	> 1800 ^f
Orion Bar	< 166 – 270 ^{h,i}	2.4 ^j	< 83 – 140 ^{i,k}
NGC 7023	50 – 120 ⁱ	31 ^j	14 ⁱ
S140	4110 ^k	3.5 – > 62 ^{j,l}	7420 ^k
NGC 2023	940 ^k	1.1 ^j	740 ^k
M17SW	2262 ^h	...	250 ^m

^a Derived from single dish data (Mauersberger & Henkel 1991; Fuente et al. 2006). See Sect. 4.1 for details.

^b Average ratio from the interferometric maps by (García-Burillo et al. 2002)

^c Average over the whole line profile in the CNB position (Usero et al. 2004).

^d Average value over the three positions in the circunuclear starburst ring with HCO detections (Usero et al. 2004).

^e From Wang et al. (2004).

^f Goicoechea et al. (2009)

^g Gerin et al. (2009)

^h Apponi et al. (1999)

ⁱ Orion Bar ionization front and PDR-peak in NGC 7023 Fuente et al. (2003)

^j Schilke et al. (2001)

^k Savage & Ziurys (2004)

^l Schenewerk et al. (1988)

^m Störzer et al. (1995)